Real-time Estimation of Lithium-ion Concentration in Both Electrodes of a Lithium-ion Battery Cell Utilizing Electrochemical-Thermal Coupling

Dey, Satadru[1]
University of California, Berkeley
Davis Hall, CA 94720, USA
satadru86@berkeley.edu

Ayalew, Beshah
Clemson University
4 Research Drive, Greenville, SC 29607, USA
beshah@clemson.edu

ABSTRACT

This paper proposes and demonstrates an estimation scheme for Li-ion concentrations in both electrodes of a Li-ion battery cell. The well-known observability deficiencies in the two-electrode electrochemical models of Li-ion battery cells are first overcome by extending them with a thermal evolution model. Essentially, coupling of electrochemical-thermal dynamics emerging from the fact that the Lithium concentrations contribute to the entropic heat generation is utilized to overcome the observability issue. Then, an estimation scheme comprised of a cascade of a sliding mode observer and an Unscented Kalman filter (UKF) is constructed that exploits the resulting structure of the coupled model. The approach gives new real-time estimation capabilities for two often-sought pieces of information about a battery cell: 1) estimation of cell-capacity, and 2) tracking the capacity loss due to degradation mechanisms such as Lithium plating. These capabilities are possible since the two-electrode model need not be reduced further to a single electrode model by adding Li conservation assumptions, which do not hold with long-term operation. Simulation studies are included for the validation of the proposed scheme. Effect of

---

[1] Corresponding author

measurement noise and parametric uncertainties are also included in the simulation results to evaluate the performance of the proposed scheme.

INTRODUCTION

Different kinds of modeling strategies have been discussed in the literature for Li-ion batteries: 1) Data-driven models [1],[2], 2) Equivalent Circuit Models [3],[4], and 3) Electrochemical models. These models are generally used for estimating State-of-Charge (SOC) and State of Health (SOH) of the batteries, which are crucial for real-time monitoring and control. Among these models, the electrochemical models arguably possess the most accurate and physically meaningful information [5]. The pseudo two-dimensional (P2D) model, which involves nonlinear partial differential equations (PDEs), is one of the benchmark models for Li-ion battery cells [6]. However, the P2D model suffers from two disadvantages: 1) too complex mathematical structure for estimator design, and, 2) high computational burden for real-time implementation. As a work around, several researchers have proposed reduced-models with less computational and structural complexity [7], [8]. The Single Particle Model (SPM) is one of such widely used reduced-models for real-time applications [9], [10].

In the SPM the electrodes are approximated as spherical particles, assuming volume-averaged current rather than distributed current in both electrodes, and also neglecting the charge and electrolyte dynamics. Several SOC estimation approaches based on SPMs have been proposed such as back-stepping PDE estimator [11], extended Kalman filter (EKF) [9], [10], nonlinear observer-based approaches presented by the

authors of the present paper [12],[13]. Another set of work resorted to adaptive estimation to simultaneously estimate the states and parameters of the model using: Particle Filter (PF) [14], unscented Kalman Filter (UKF) [15], Iterative EKF (IEKF) [16], adaptive PDE observer [17] and nonlinear geometric observer [18]. The authors of the present paper also contributed to this segment by proposing sliding mode observer [19] and nonlinear adaptive observer [20], [35].

From estimation theory viewpoint, the two-electrode SPM suffers a drawback where the Li-ion concentration states are weakly observable from the differential voltage measurement [10]. One of the main reasons for that is the Li-ion concentration states of the electrodes are coupled in the voltage output through their thermodynamic potentials, whereas their dynamics are decoupled. To resolve this observability issue the existing estimation schemes approximate one electrode's concentration state as a function of the concentration state of other electrode [10],[11],[12]. This approximation results in a one-electrode SPM (either anode or cathode) with strong observability of the corresponding states from the voltage measurement. However, this afore-mentioned algebraic function, and hence the approximation, comes from the underlying assumption of the conservation of the total number of Li-ions in the cell. This assumption may not be true as there are losses of Li-ions due to aging and other phenomena over persistent long-term operation.

In light of the above discussion, the main contribution of this work is: we relaxed the aforementioned assumption (conservation of the total number of Li-ions in the cell) and designed an estimation scheme based on the two-electrode SPM. Essentially, the

main difference between previously proposed battery state estimation schemes [9-20, 35] and the current work is that previous schemes estimate the overall cell SOC based on the Li-ion conservation assumption, whereas the current work relaxes such assumption and estimates the SOC (Li-ion concentration) of individual electrodes. Estimates of individual electrode SOC would enable additional crucial benefits/features such as health monitoring of individual electrodes, capacity tracking of the cell and detection of mechanisms leading to loss of active Lithium, e.g. Li plating.

In doing so, we first showed that the observability of both electrode concentration states can be improved by exploiting the electrochemical-thermal coupling. This arises from the fact that the electrochemical parameters of the cell and the thermodynamic potential of the electrodes depend on the temperature. On the other hand, electrode surface concentrations contribute to the heat generation in the thermal model. In the estimation scheme, we used a cascaded two-observer structure that exploits this coupling. Observer I is a sliding mode observer which is used to estimate the heat generation term contributed by the electrode concentration states. Then, this estimate of the heat-generation term is fed to Observer II as a pseudo-measurement. Observer II, which is based on the two-electrode SPM, uses this pseudo-measurement and the differential voltage measurement to estimate the electrode concentration states. The design of Observer II is based on an Unscented Kalman filter (UKF) framework that can account for the model nonlinearities and uncertainties.

A preliminary version of this work was presented in [34]. In the present paper, we extend our preliminary work [34] by including: 1) Discussion and results of the

application of the scheme to estimate initial capacity of the cell as well as the capacity degradation over time; 2) Detection scheme for degradation mechanisms such as lithium plating in cells; 3) Additional simulation results under varying operating conditions such as dynamic discharge profiles; and, 4) Discussions and simulation studies on the effect of the modeling uncertainties and measurement noises on the scheme. It is shown that the proposed estimation scheme is able to estimate Li-ion concentration states in both electrodes from measured cell voltage, temperature and current. Further, it is shown how the estimation of individual electrode concentrations can be used to compute the real-time capacity of the cell and to help in detecting combinations of degradation mechanisms leading to loss of Lithium in the cell.

The organization of the paper is as follows: First, we review the SPM and thermal model for Li-ion cell. Next, a detailed discussion of the system observability is provided. Then the estimation scheme and its design are presented. This is followed by the application of the proposed scheme for two specific objectives: capacity tracking and Lithium plating detection. Then, simulation results are provided for the performance of the scheme along with the effects of modeling, parametric and measurement uncertainties. Lastly, the paper is concluded with some remarks.

MODELING OF LITHIUM-ION CELL

The SPM is derived from the P2D model [6] by assuming volume-averaged current and neglecting electrolyte and charge dynamics. We shall use the schematic given in Fig. 1 and notations given in the nomenclature section for the SPM equations.

The two diffusion PDEs of the SPM describing the Li-ion diffusion dynamics are [9], [10]:

$$\frac{\partial c_s^\pm}{\partial t} = \frac{D_s^\pm(T)}{r^2}\frac{\partial}{\partial r}\left(r^2\frac{\partial c_s^\pm}{\partial r}\right)$$

$$\left.\frac{\partial c_s^\pm}{\partial r}\right|_{r=0} = 0, \qquad \left.\frac{\partial c_s^\pm}{\partial r}\right|_{r=R^\pm} = \frac{\pm I}{a_s^\pm F D_s^\pm(T)AL^\pm} \tag{1}$$

where $c_s^\pm$ is the Li-ion concentration of the electrodes, I is charge/discharge current and $a_s^\pm = 3\varepsilon^\pm/R^\pm$ with $\varepsilon^\pm$ are the solid phase volume fractions of each electrode. The output voltage can be written as:

$$V = \frac{\bar{R}T}{\alpha^+ F}sinh^{-1}\left(\frac{I}{2a_s^+ AL^+ i_0^+}\right)$$

$$-\frac{\bar{R}T}{\alpha^- F}sinh^{-1}\left(\frac{I}{2a_s^- AL^- i_0^-}\right) + U^+\left(c_{s,e}^+,T\right) - U^-\left(c_{s,e}^-,T\right) - R_f(T)I \tag{2}$$

where $i_0^\pm$ are the exchange current densities given by:

$$i_0^\pm = k_0^\pm(T)\sqrt{c_e c_{s,e}^\pm\left(c_{s,max}^\pm - c_{s,e}^\pm\right)} \tag{3}$$

Further, to capture the temperature dynamics, the following thermal model [21] is considered:

$$mC_p \frac{dT}{dt} = I\left(U^+(c_{s,e}^+, T) - U^-(c_{s,e}^-, T) - V - T\left(\frac{\partial U^+}{\partial T} - \frac{\partial U^-}{\partial T}\right)\right) - hA_s(T$$

$$- T_\infty) \tag{4}$$

where T is the temperature and $\frac{\partial U^\pm}{\partial T}$ are functions of the surface concentrations $c_{s,e}^\pm$.

Further, the solid phase diffusion coefficients ($D_s^\pm$), the contact film resistance (R_f) and

the reaction rate constants ($k_0^\pm$) are functions of temperature based on the Arrhenius

relationship [21]:

$$k_0^\pm(T) = k_{0,ref}^\pm exp\left(\frac{E_K^\pm}{\bar{R}}\left(\frac{1}{T} - \frac{1}{T_{ref}}\right)\right)$$

$$D_s^\pm(T) = D_{s,ref}^\pm exp\left(\frac{E_{Ds}^\pm}{\bar{R}}\left(\frac{1}{T} - \frac{1}{T_{ref}}\right)\right)$$

$$R_f(T) = R_{f,ref} exp\left(\frac{E_R}{\bar{R}}\left(\frac{1}{T} - \frac{1}{T_{ref}}\right)\right) \tag{5}$$

where T_{ref} is the reference temperature at which $k_{0,ref}^\pm$, $D_{s,ref}^\pm$ and $R_{f,ref}$ are

evaluated.

Note: As noted in the existing literature, the predictive ability of the SPM degrades high

charge-discharge rates, especially when the electrolyte dynamics have significant

contributions. The extensions of the SPM with electrolyte dynamics and thermal models

are also proposed in [22] and [23] which improve the predictive ability. However, the

objective of this paper is to illustrate the observability and estimation concept using the

conventional two-electrode SPM along with the averaged thermal model. Extension of

our design based on such extended SPM models can be considered in future work.

Furthermore, the model inaccuracy of the SPM is compensated to a certain extent by the use of Unscented Kalman Filter (UKF) algorithm, which will be detailed later.

Next, we approximate the PDEs in (1) to a set of ODEs (6)-(7), using a finite difference method where the spatial domain is discretized into (M+1) nodes (see Fig. 1).

Negative electrode:

$$\dot{c}_{sN0} = -3a_N c_{sN0} + 3a_N c_{sN1}$$

$$\dot{c}_{sNm} = \left(1 - \frac{1}{m}\right) a_N c_{sN(m-1)} - 2a_N c_{sNm} + \left(1 + \frac{1}{m}\right) a_N c_{sN(m+1)}$$

$$\dot{c}_{sNM} = \left(1 - \frac{1}{M}\right) a_N c_{sN(M-1)} - \left(1 - \frac{1}{M}\right) a_N c_{sNM} - \left(1 + \frac{1}{M}\right) b_N I \tag{6}$$

Positive electrode:

$$\dot{c}_{sP0} = -3a_P c_{sP0} + 3a_N c_{sP1}$$

$$\dot{c}_{sPm} = \left(1 - \frac{1}{m}\right) a_P c_{sP(m-1)} - 2a_P c_{sPm} + \left(1 + \frac{1}{m}\right) a_P c_{sP(m+1)}$$

$$\dot{c}_{sPM} = \left(1 - \frac{1}{M}\right) a_P c_{sP(M-1)} - \left(1 - \frac{1}{M}\right) a_P c_{sPM} - \left(1 + \frac{1}{M}\right) b_P I \tag{7}$$

where $m = 1, \dots, (M-1)$, $[c_{sP0}, c_{sP1}, \dots c_{sPM}]$ and $[c_{sN0}, c_{sN1}, \dots c_{sNM}]$ are Li-ion concentration states, $\Delta_N = R^-/M$, $\Delta_P = R^+/M$, $a_N = D_s^-(T)/\Delta_N^2$, $a_P = D_s^+(T)/\Delta_P^2$, $b_N = 1/a_s^- F \Delta_N AL^-$, $b_P = 1/a_s^+ F \Delta_P AL^+$.

Substituting $c_{s,e}^- = c_{sNM}$ and $c_{s,e}^+ = c_{sPM}$ in (2), the voltage expression becomes:

$$V = \frac{\bar{R}T}{\alpha^+ F} sinh^{-1}\left(\frac{I}{2a_s^+ AL^+ i_0^+}\right)$$

$$- \frac{\bar{R}T}{\alpha^- F} sinh^{-1}\left(\frac{I}{2a_s^- AL^- i_0^-}\right)$$

$$+ U^+(c_{sPM}, T) - U^-(c_{sNM}, T) - R_f(T)I \tag{8}$$

where $i_0^{\pm}$ are the exchange current densities given by:

$$i_0^+ = k_0^+(T)\sqrt{c_e c_{sPM}\left(c_{s,max}^- - c_{sPM}\right)}$$

$$i_0^- = k_0^-(T)\sqrt{c_e c_{sNM}\left(c_{s,max}^- - c_{sNM}\right)} \qquad (9)$$

Note: In this work, a finite difference method is adopted to reduce the PDE model to ODE model. However, several other methods exist that can be used for this model reduction in the proposed scheme [36].

OBSERVABILITY ANALYSIS

Observability of Li-ion Concentrations in both Electrodes from only Voltage Output (Conventional SPM):

Following from above, the electrode concentration dynamics and the voltage output can be written in the following state-space form:

$$\begin{bmatrix} \dot{x}_P \\ \dot{x}_N \end{bmatrix} = \begin{bmatrix} A_P & 0_M \\ 0_M & A_N \end{bmatrix}\begin{bmatrix} x_P \\ x_N \end{bmatrix} + \begin{bmatrix} B_P \\ B_N \end{bmatrix} u$$

$$y_V = U_P(x_{PM}, T) - U_N(x_{NM}, T) + n_P(x_{PM}, T) - n_N(x_{NM}, T) - R_f(T)u \qquad (10)$$

where $x_P = [c_{sP1}, \dots c_{sPM}]^T \in R^M$ and $x_N = [c_{sN1}, \dots c_{sNM}]^T \in R^M$, $u \in R$ is input current, $y_V = V \in R$ is the output voltage, $x_{PM} = c_{sPM} \in R$ and $x_{NM} = c_{sNM} \in R$ are the surface concentration states, $A_P \in R^{M\times M}$ and $A_N \in R^{M\times M}$ are temperature dependent tri-diagonal matrices obtained from the state matrices in (6) and (7) respectively, $0_M \in R^{M\times M}$ is the zero matrix, $B_P \in R^{M\times 1}$ and $B_N \in R^{M\times 1}$ are the input matrices derived from (6) and (7) respectively, $U_P = U^+ : R^2 \to R$ and $U_N = U^- : R^2 \to R$ are the temperature dependent open-circuit potential maps for the positive and

negative electrode, respectively, $R_f \in R$ is the temperature dependent scalar film resistance, $n_P: R^2 \to R$ and $n_N: R^2 \to R$ are the first two scalar over-potential terms in (8), respectively.

Around a given nominal operating temperature $T = T^*$, the observability of (10) is studied in [10] where the states are found to be weakly observable from the voltage output. This unobservability can also be explained by considering the system structure of (10). There is no coupling between individual electrode concentration states in (10) i.e. A_P and A_N have no common terms. However, in the nonlinear output voltage map y_V, the electrode surface concentrations x_{PM} and x_{NM} are coupled via their thermodynamic potential. This leads to the afore-mentioned unobservability. Two solutions have been presented in literature to improve on this concern before undertaking estimator design: 1) In [10], the surface concentration of the negative electrode is approximated as a function of the positive electrode surface concentration using the stoichiometry ratio; 2) In [11], the opposite approximation is done under the assumption of the conservation of the total number of Li-ions in the cell. However, the conservation assumption may not be true as discussed before. In this paper, we take a different approach where we improve the observability by adding the thermal model to the two-electrode SPM (10).

Observability of Li-ion Concentrations in both Electrodes from Voltage and Temperature Output (Conventional SPM with Thermal Dynamics):

With the addition of thermal dynamics, the Lithium-ion cell model can be written as:

$$\begin{bmatrix} \dot{x}_P \\ \dot{x}_N \end{bmatrix} = \begin{bmatrix} A_P & 0_M \\ 0_M & A_N \end{bmatrix} \begin{bmatrix} x_P \\ x_N \end{bmatrix} + \begin{bmatrix} B_P \\ B_N \end{bmatrix} u$$

$$mC_p \dot{T} = u\{U_P(x_{PM}, T) - U_N(x_{NM}, T) - y_V\}$$

$$-uT\{U_P^D(x_{PM}) - U_N^D(x_{NM})\} - hA_s(T - T_\infty)$$

$$y_V = U_P(x_{PM}, T) - U_N(x_{NM}, T) + n_P(x_{PM}, T) - n_N(x_{NM}, T) - R_f(T)u$$

$$y_T = T \tag{12}$$

where $U_P^D = \dfrac{\partial U^+}{\partial T} : R \to R$ and $U_N^D = \dfrac{\partial U^-}{\partial T} : R \to R$ are functions of x_{PM} and x_{NM},

respectively, and $y_T = T \in R$ is the measured temperature. It can be seen from (12)

that the thermal model possess additional information about the electrode surface

concentrations in the form of $\{U_P^D(x_{PM}) - U_N^D(x_{NM})\}$. This is the crucial feature behind

the improvement of the observability of the concentration state in both electrodes.

Next, we verify the observability using the sufficient rank condition for the local

nonlinear observability notion described in [24]:

$$O(x^*, u^*) = \begin{bmatrix} \dfrac{\partial}{\partial x}(L_f^0[h]) \\ \vdots \\ \dfrac{\partial}{\partial x}(L_f^{2M-1}[h]) \end{bmatrix}_{x=x^*, u=u^*}$$

where $h = [y_V \quad y_T]^T$ represents the output voltage map, $x = [x_P^T, x_N^T]$ represents the

state vector and u represents the input current. The observability of (12) depends on

the functions U_P, U_N, U_P^D and U_N^D, which are specific to different Li-ion battery

chemistries. Here, we consider the LiCoO2-Graphite chemistry for illustration. The

functions U_P, U_N, U_P^D and U_N^D for this chemistry are shown in Fig. 2. The rank of the

observability matrix O is checked at different operating points with a 4-node

discretization for each electrode particle. Therefore, the dimension of the state vector is 7 (3 concentration states for each electrode and one thermal state). It is noted that the observability matrix O has rank 7 at all tested operating points (MATLAB 2013a, 32 bit), except for the operating points with $u^* = 0$. Therefore, it can be concluded that the system (12) is locally observable for all of the operating points tested except for $u^* = 0$.

Remark I: In case of $u^* = 0$, thermal dynamics does not carry any information of the Li-ion concentration states. Hence, the system loses its observability. This is evident from the expression of the thermal dynamics in (12).

Remark II: Considering Fig. 2, it can be noted that the values of U_P^D and U_N^D are much smaller than that of U_P and U_N and are generally in the mV range. However, U_P^D and U_N^D enter the thermal dynamics equation (4) as uTU_P^D and uTU_N^D where T is the temperature in K and u is the current in A. Considering the nominal temperature around 298 K and the nominal current around 10 A, U_P^D and U_N^D are amplified by the factor of 2980 which makes them comparable to the amplitudes of U_P and U_N. Therefore, the measurements of voltage, current and temperature should be sufficiently accurate in order to observe the states through these terms. This is one of the limitations of using this model for estimation.

Remark III: Another observation that can be made from Fig. 2 is that the U_N^D function becomes flat after x_{NM}/x_{NM-max} crosses 0.5. This indicates the insensitivity of U_N^D to the negative electrode surface concentration state in the region $0.5x_{NM-max}$ to x_{NM-max}. However, this does not lead to the unobservability of the negative electrode

concentration as the other three functions the U_P^D, U_P and U_N are still sensitive to the corresponding states in that region. This makes the overall system still observable.

ESTIMATION SCHEME

The estimation scheme is depicted in Fig. 3.

As can be seen from Fig. 3, the scheme has two observers running in cascade.

Observer I: This is designed based on the thermal model of the system. This observer estimates a pseudo-measurement (y_{pseudo}) signal using the current and temperature measurement. This y_{pseudo} essentially contains the electrode concentration function that contributes to the heat generation term.

Observer II: This is designed based on the two-electrode SPM. This observer estimates Li-ion concentration states in both electrodes using the voltage and the pseudo-measurement (y_{pseudo}) signal.

Details of Observer I

The design of Observer I is done based on sliding-mode observer theory [25]. The observer structure is given below:

$$mC_p\dot{\hat{T}} = -uy_V - hA_s(\hat{T} - T_\infty) + L_T sgn(T - \hat{T}) \tag{13}$$

where y_V and T are the measured voltage and temperature and L_T is the observer gain to be determined. Subtracting (13) from the thermal dynamics in (12), the error dynamics can be written as:

$$mC_p\dot{\tilde{T}} = u\{U_P(x_{PM}, T) - U_N(x_{NM}, T)\}$$

$$-uT\{U_P^D(x_{PM}) - U_N^D(x_{NM})\} - hA_s(\tilde{T}) - L_T sgn(\tilde{T}) \tag{14}$$

where $\tilde{T} = T - \hat{T}$ is the estimation error. We analyze the error dynamics by choosing

the Lyapunov function candidate $V_T = 0.5mC_p\tilde{T}^2$. The derivative becomes:

$$\dot{V}_T = mC_p\tilde{T}\dot{\tilde{T}} = [u\{U_P(x_{PM}, T) - U_N(x_{NM}, T)\}$$

$$- uT\{U_P^D(x_{PM}) - U_N^D(x_{NM})\}]\tilde{T} - hA_s\tilde{T}^2 - L_T\tilde{T}sgn(\tilde{T})$$

$$\Rightarrow \dot{V}_T \leq |\tilde{T}|\{|u||U_P(x_{PM}, T) - U_N(x_{NM}, T)| + |u||T||U_P^D(x_{PM}) - U_N^D(x_{NM})|$$

$$- L_T\} \tag{15}$$

<u>Design of observer gain:</u> Note that from (15), a high value of the observer gain satisfying

the following condition:

$$L_T > F_{max} \triangleq |u|_{max}|U_P(x_{PM}, T) - U_N(x_{NM}, T)|_{max} + |u|_{max}|T|_{max}|U_P^D(x_{PM}) -$$

$$U_N^D(x_{NM})|_{max} > 0 \; \forall t,$$

will result in $\dot{V}_T < 0$. For design purposes, the following values can be selected:

$|u|_{max}$: This can be determined a priori based on the operating maximum input current.

$|T|_{max}$: This can be determined a priori based on the maximum possible temperature

range for the battery operation.

$|U_P(x_{PM}, T) - U_N(x_{NM}, T)|_{max}$, $|U_P^D(x_{PM}) - U_N^D(x_{NM})|_{max}$: These values can be

determined apriori based on the particular electrode chemistries.

Considering the observer gain satisfies the above condition, the V_T dynamics can

be written as:

$$\dot{V}_T \leq -\beta\sqrt{V_T}, with \; \beta = (L_T - F_{max}) > 0 \tag{16}$$

$$\Rightarrow V_T < \left(-\frac{\beta}{2}t + \sqrt{V_T(t=0)}\right)^2$$

Therefore, it can be concluded from (16) that V_T and the estimation error $\left|\tilde{T}\right|$ will converge to the sliding surface $s_T = \tilde{T} = 0$ in a finite time given by $t_f \leq 2\sqrt{V_T(t=0)}/$ β. Furthermore, on the sliding surface, we have the following conditions satisfied: $s_T = \tilde{T} = 0$ and $\dot{s}_T = \dot{\tilde{T}} = 0$ [25]. Considering these conditions, the error dynamics (14) can be re-written as:

$$0 = u\{U_P(x_{PM}, T) - U_N(x_{NM}, T)\}$$

$$-uT\{U_P^D(x_{PM}) - U_N^D(x_{NM})\} - v_T \tag{17}$$

where v_T is the equivalent output error injection signal required to maintain the sliding motion. It is a continuous approximation (or filtered version) of the switching signal $L_T sgn(\tilde{T})$. For real-time implementation, v_T can be extracted by passing the switching signal $L_T sgn(\tilde{T})$ through a low-pass filter [25]. To this end, the pseudo-measurement signal can be extracted from (17) as given below:

$$y_{pseudo} = v_T = u\{U_P(x_{PM}, T) - U_N(x_{NM}, T)\}$$

$$-uT\{U_P^D(x_{PM}) - U_N^D(x_{NM})\} \tag{18}$$

Details of Observer II

The design of Observer II is based on the Unscented Kalman Filter (UKF) framework [26]. UKF is developed from the widely used Extended Kalman Filter (EKF)

approach for nonlinear systems [27]. The main advantage of UKF lies in the fact that it can accommodate nonlinearities of the system along with the modeling and measurement uncertainties. UKF follows the same prediction-correction steps as any Kalman filtering approach. However, instead of applying the Jacobian of the nonlinear functions and thereby linearizing the system for gain calculation as in EKF, UKF applies the unscented transform that keeps the model nonlinearities. The system model used for the design of Observer II is the two-electrode concentration dynamics (12) with the output information of y_{pseudo} from the Observer I and measured voltage y_V. To apply the UKF approach in the present case, the continuous-time system is transformed into a discrete-time system using Euler's discretization with sample time T_s, which results in the following discrete time state-space model:

$$\begin{bmatrix} \bar{x}_P(k+1) \\ \bar{x}_N(k+1) \end{bmatrix} = \begin{bmatrix} \bar{A}_P(k) & 0_M \\ 0_M & \bar{A}_N(k) \end{bmatrix} \begin{bmatrix} \bar{x}_P(k) \\ \bar{x}_N(k) \end{bmatrix} + \begin{bmatrix} \bar{B}_P(k) \\ \bar{B}_N(k) \end{bmatrix} u(k)$$

$$Y(k) = \begin{bmatrix} \bar{y}_V(k) \\ \bar{y}_{pseudo}(k) \end{bmatrix} = \begin{bmatrix} h_1\big(T(k), \bar{x}_P(k), \bar{x}_P(k), u(k)\big) \\ h_2\big(T(k), \bar{x}_P(k), \bar{x}_P(k), u(k)\big) \end{bmatrix} \qquad (19)$$

where $\bar{x}_P$ and $\bar{x}_N$ are discrete-time states, $\bar{y}_V$ and $\bar{y}_{pseudo}$ are the discrete-time outputs, $\bar{A}_P, \bar{A}_N, \bar{B}_P, \bar{B}_N$ are the nonlinear matrices derived from the dynamic equations of (12) via Euler's discretization and h_1, h_2 are the time-varying functions derived from the output equations y_V in (12) and y_{pseudo} in (18). Note that, the nonlinearity is due to the dependency of the matrices and functions on the temperature. Especially, the matrices $\bar{A}_P$ and $\bar{A}_N$ are functions of the temperature due to the solid phase diffusion coefficient's Arrhenius dependence on temperature, as shown in (5). However, we assume that these matrices are computed online using temperature measurement and

treated as known time-varying matrices in the estimator. The system (19) can be written in compact from as:

$$x(k + 1) = A(k)x(k) + B(k)u(k) + q(k)$$

$$y(k) = h\big(k, x(k), u(k)\big) + \bar{r}(k) \tag{20}$$

where q represents the process noise accounting for the un-modeled dynamics, modeling and parametric uncertainties; $\bar{r}$ represents the measurement inaccuracies and unmodeled output uncertainties. The corresponding process and measurement noise covariance matrices are Q and R. The covariance of the state estimation is P_x. The UKF implementation follows the steps given in [27].

APPLICATIONS

Cell Capacity Estimation

Here we present one important application of the proposed scheme: the capacity estimation/tracking for the cell. Following the approach in [11], the total number of Li-ions in the cell can be calculated as:

$$n_{Li} = \frac{\varepsilon_s^+ L^+ A}{\frac{4}{3}\pi(R^+)^3} \int_0^{R^+} 4\pi r^2 c_s^+(r, t)dr + \frac{\varepsilon_s^- L^- A}{\frac{4}{3}\pi(R^-)^3} \int_0^{R^-} 4\pi r^2 c_s^-(r, t)dr \tag{21}$$

Note that, n_{Li} essentially represents the capacity of the cell by calculating usable Li-ions amount and hence can be served as a capacity indicator of the cell. Using the formula in (21) and the electrode concentration estimates from Observer II, the capacity indicator can be estimated as:

$$\hat{n}_{Li} = \frac{\varepsilon_s^+ L^+ A}{\frac{4}{3}\pi(R^+)^3} 4\pi\Delta_P^3 \sum_{i=1}^{M} i^2 \hat{c}_{sPi} + \frac{\varepsilon_s^- L^- A}{\frac{4}{3}\pi(R^-)^3} 4\pi\Delta_N^3 \sum_{i=1}^{M} i^2 \hat{c}_{sNi}$$

(22)

Note that aging and other phenomenon of the cell will result in loss of cycle-able Li-ions over persistent long-term operations and hence the value of the parameter $\hat{n}_{Li}$ will decrease with time.

Lithium Plating Detection

In this part, we will illustrate Lithium plating detection as another application of the estimated Li-ion concentrations in positive and negative electrode. Lithium plating happens during charging the Li-ion cell and essentially results in deposition of metallic Lithium on the graphite anode. Several factors such as electrolyte characteristics, ratio between negative and positive electrode capacities, charging rates etc affect the negative electrode kinetics and Li-ion diffusion rates in such a way that Lithium is deposited on the negative electrode instead of intercalating the negative electrode [28], [29]. This mechanism may degrade the Li-ion cell performance and safety.

To detect Lithium plating, we adopt the approach in [30] where the Li-ions transport rates in and out of the electrodes were used as indicators of the same. However, the approach given in [30] was based on two-electrode models with only output voltage, which suffers the previously mentioned unobservability. In this paper, we overcome this limitation by using our extended model and cascaded observers.

As shown in [31], the insertion and extraction rates of the Li-ions follow the diffusion dynamics and hence they can be written as:

$$E_P = \left| \frac{\partial c_{P-avg}}{\partial t} \right|, I_N = \left| \frac{\partial c_{N-avg}}{\partial t} \right| \qquad (23)$$

where E_P and I_N are the Li-ion extraction rate from positive electrode and insertion rate into negative electrode, c_{P-avg} and c_{N-avg} are the volume-averaged Li-ion concentrations in the positive and the negative electrodes, respectively, and given as:

$$c_{P-avg} = \frac{1}{\frac{4}{3}\pi(R^+)^3} \int_0^{R^+} 4\pi r^2 c_s^+(r,t)dr$$

$$c_{N-avg} = \frac{1}{\frac{4}{3}\pi(R^-)^3} \int_0^{R^-} 4\pi r^2 c_s^-(r,t)dr \qquad (24)$$

The plating phenomenon is detected when the extraction rate E_P exceeds the maximum possible extraction rate (E_{P-max}) and I_N drops below the minimum possible insertion rate (I_{N-min}). These limits can be obtained in the following way: Collect E_P and I_N data from the healthy battery either by 1) Monte-Carlo simulation studies on the battery model on varying different operating conditions, different levels of measurement noise, different levels of modeling uncertainties, or, 2) Experimental studies on a physical battery under different operating conditions [33]. Then, choose the maximum and minimum of E_P and I_N as the limits.

RESULTS AND DISCUSSIONS

To validate the proposed estimation scheme, we perform simulation studies in this section. For simulation purpose, battery cell model parameters of a 6.8 Ah LiCoO2-Graphite cell are taken from [32]. The plant model used for this purpose is a two-electrode SPM with averaged thermal dynamics. However, to verify the convergence, the Observer II is initialized with incorrect initial conditions. As the temperature is measured, we initialize the Observer I with the correct initial condition. In the simulation scenarios, we start with verifying the performance with smaller measurement noise level. Then gradually we inject higher levels of measurement noise and parametric uncertainties to verify the effectiveness of the scheme.

State and Capacity Estimation

In this section, we present simulation scenarios where the measured variables from the plant model are injected with zero mean Gaussian noise 1 mV, 1 mA and 0.1°C.

Constant Current Discharge:

The estimation performance under a constant 1C current discharge is shown in Fig. 4 through Fig. 7. In Fig. 4, the output estimation performance is shown, which validates that the cascade of observer I and II is able to track the temperature and voltage with sufficient accuracy. Figures 5 and 6 show the reasonable performance in estimation of the surface and bulk SOC for both electrodes. Bulk SOC represents the volume-averaged combination of the Li-ion concentration state variables. In Fig. 7, the

performance of observer I is shown in estimating the pseudo-measurement. Moreover, Fig. 7 also shows the estimation of capacity indicator n_{Li}, which is accurately estimated in a few minutes.

Dynamic Discharge (UDDS-type profile):

In the next study, we show the estimation performance under a dynamic discharge profile in Fig. 8. The current profile is generated from a scaled-down version of the UDDS velocity profile. Moreover, a bias component is added to avoid the zero-current limitation mentioned earlier. It is evident that the observer-based scheme estimates the bulk SOC and the capacity indicator with reasonable accuracy.

Comparison

In this study, we compare the estimation performance of the scheme using the two-electrode formulation proposed in this work against a similar estimation scheme that only uses a single-electrode formulation using the assumption of conservation of total number of Li-ions in the cell. The second estimation scheme is an UKF designed based on only the positive electrode concentration dynamics and voltage output. In the simulation plant model, we have injected a side reaction current component which leads to capacity fade with time. The result of the estimation performance is shown in Fig. 9. It is evident that the estimate from the scheme with conservation assumption diverges from the actual value with time while the proposed scheme is able to track with reasonable accuracy.

Capacity Fade Tracking

Here we illustrate the observer's performance in tracking the capacity fade of the battery cell under 1C discharge scenario. The capacity fade is simulated by adding a side reaction current component into the plant model which is not known to the estimators. The performance of the capacity fade tracking is shown in Fig. 10.

Lithium Plating Detection

In this section, we illustrate the observer's performance in Lithium plating detection. The simulation scenario used for this case study is C/10 charging at ambient temperature -20°C. To illustrate the Lithium plating condition in simulation scenario, we have injected a step-like additive C/5 charging input current component to the positive electrode of the plant-model. This additive input current causes a sudden change in current density in the positive electrode while the current density in the negative electrode is kept constant. This essentially represents a loss in active Lithium-ions, as the Li-ion extraction rate from the positive electrode would be higher than the insertion rate in the negative electrode. In this case study, the positive electrode current density is increases at t=600 sec. The bulk SOC estimation performance is shown in Fig. 11 where the observer-based scheme is able to track the bulk SOC even after the occurrence of the plating. Further, the plating detection signals E_P and I_N are shown in Fig. 12. It can be seen that E_P crosses the maximum limit after the plating has occurred and hence the plating is successfully detected.

Note: The case study of Lithium plating is used to illustrate the capability of the scheme for detecting any mechanism that leads to loss of Lithium in the cell which in turn results in capacity loss. Loss of Lithium can be interpreted as: the total amount of Li-ion leaving one electrode is not reaching the other electrode; some of them are lost due to undesirable reactions. Lithium plating is one of such scenario. Therefore, any such mechanism that results in loss of Lithium can be detected by the estimation scheme. So, the reversible plating cannot be detected by the proposed scheme as it does not cause capacity loss. On the other hand, reversible plating which causes capacity loss will be detected by the scheme. Furthermore, the detection accuracy depends on the modeling and measurement uncertainties. The loss of Lithium due to plating must be sufficiently high such that the Lithium extraction rate goes beyond the pre-defined limit E_{Pmax}.

Estimation Performance Under the Effect of Uncertainties

Here, we study the robustness properties of the estimation scheme under different uncertainties. These studies are conducted under 1C discharge scenario.

<u>Effect of measurement noise and bias</u>

It was mentioned in the design section that this scheme is sensitive to measurement noise. In this section, we study the effect of measurement noise via simulation by injecting different noise levels in the all three measurements (voltage, temperature and current). It is found that the scheme generates reasonable estimates approximately up to 25 mV voltage measurement noise and 50 mA current measurement noise. Above those ranges, the steady-state estimation error goes

significantly higher reducing the effectiveness of the scheme. Other than measurement noise, measurement bias is also considered. For voltage and current measurements, it is noted that the scheme performs satisfactorily up to 5 mV and 12 mA measurement bias. Beyond these values, the performance of the scheme degrades.

Another interesting point is noted in simulation studies regarding the temperature measurement noise. Above 0.5^oC noise level in the temperature measurement the estimates tend to diverge after a certain point when the signal-to-noise ratio gets smaller. One such scenario is shown in Fig. 13. This is because of the reason that in high temperature measurement noise, the sliding surface deviates significantly from $\tilde{T} = 0$ and settles to $s_T = \tilde{T} = \eta$, where η is the lumped effect of temperature measurement noise. This creates a significant bias in pseudo-measurement which the UKF is unable to handle. Similar effects have been noted under temperature measurement bias where the estimation performance degrades beyond 0.1^oC bias.

Effect of parametric uncertainties

In this section, we study the estimation performance under parametric uncertainties. The plant model observer is initialized with incorrect parameter values. We chose the following parameters for this study: $D_{s,ref}^-$, $D_{s,ref}^+$, a_s^-, a_s^+, $R_{f,ref}$, h and C_p. The observer is initialized with 50% error in one of these parameters in each case. It is noted that the scheme performs well with reasonable accuracy in case of uncertainties in $D_{s,ref}^-$, $D_{s,ref}^+$, a_s^-, a_s^+. The steady-state errors for these parametric uncertainties are shown in Table 1. Note that, the capacities of individual electrodes can

be written as: $Q^\pm = \varepsilon^\pm A L^\pm F c_{s,max}^\pm |y_{100\%} - y_{0\%}|$ where $y_{0\%}$ and $y_{100\%}$ are the stoichiometry points of the individual electrode [37]. Further, the definition $a_s^\pm = 3\varepsilon^\pm / R^\pm$ (see after (1)) indicates that 50% uncertainty injection in $a_s^\pm$ is essentially equivalent to 50% uncertainty injection in $\varepsilon^\pm$ which in turn injects uncertainty in the individual electrode capacities $Q^\pm$. Therefore, it can be concluded that the scheme performs reasonably under the deviation of individual electrode capacities due aging.

However, the scheme is found to be sensitive to the parametric variations in $R_{f,ref}$, h and C_p. Estimation error for the bulk SOC is shown in Fig. 14. It can be seen that the negative electrode bulk SOC estimation is degraded in case of any of these parameter variations. However, for positive electrode case, it is still reasonable in case of uncertainties in $R_{f,ref}$ and h but degrades significantly in case of C_p uncertainty. The reason behind this is that in the voltage measurement expression, the contribution of the positive electrode concentration is significantly higher than that of the negative electrode concentration. Therefore, any smaller uncertainties in the voltage expression such as deviation in $R_{f,ref}$ make the negative electrode estimation poor. However, the uncertainty in C_p affects the pseudo-measurement estimation significantly and therefore affects estimation of the concentration in both electrodes.

Estimation Performance Under Zero Input Current

In the final simulation, we show the performance of the scheme under zero current. As discussed and showed in the observability analysis, the model loses observability under zero input current due to the absence of the heat generation term.

It is confirmed in the result shown in Fig. 15 where the input current is made to zero at 1000 sec and the estimation errors diverge to a different non-zero value. So, it is important to engage the proposed estimation scheme under some non-zero current.

Note: The limitations of this approach are: 1) addition of the temperature measurement for each cell increases the hardware cost to some extent, 2) a one-state thermal dynamic model needs to be solved in Observer I. However, the gain from the additions of the model and measurement is the availability of the estimates of each electrode states, which can be used for battery health monitoring (e.g. capacity tracking, plating detection) as detailed in the previous sections.

CONCLUSION

In this paper, we present an estimation scheme to estimate Li-ion concentrations in the negative and positive electrodes of the Li-ion cell. To capture the battery internal physics, we adopt the two-electrode electrochemical SPM along with averaged thermal dynamics for the observer design. First, the improvement of the observability of the Li-ion concentration states in both electrodes is given measurement of temperature and voltage. Next, the details of the cascaded observer structure are outlined. The first observer estimates a function containing Li-ion surface concentration information from the thermal dynamics and the measured temperature. The second observer uses this information along with the measured voltage to estimate the Li-ion concentration states of both electrodes. Two important applications of the proposed estimation scheme are

presented: cell capacity estimation and Lithium plating detection. The effectiveness of the scheme is verified by simulation studies. Furthermore, the effect of measurement noise and parametric uncertainties are evaluated.

However, there are some aspects that should be explored as future work of this study. First, the scheme is illustrated using particular battery chemistry (LiCoO2-Graphite). The effectiveness of the scheme should be explored for other chemistries. Next, solutions should be investigated to deal with the sensitivity to high noise levels in the measurements. Finally, the proposed scheme should be validated using experimental data to verify its effectiveness.

FUNDING

NOMENCLATURE

A	Current collector area (cm^2)
A_s	Surface area of the cell (cm^2)
$a_s^{\pm}$	Electrode surface area, specific (cm^2/ cm^3)
c_e	Li-ion concentration, electrolyte phase (mol/cm^3)
$c_s^{\pm}$	Li-ion concentration, solid phase (mol/cm^3)
$c_{s,e}^{\pm}$	Li-ion surface-concentration, solid-phase (mol/cm^3)
$c_{s,max}^{\pm}$	Li-ion max. concentration, solid-phase (mol/cm^3)
$D_s^{\pm}$	Solid-phase diffusion coefficient (cm^2/s)
$D_{s,ref}^{\pm}$	Solid-phase diffusion coefficient at T_{ref} (cm^2/s)
$E_K^{\pm}$	Diffusion coefficient activation energy (J/mol)
$E_{Ds}^{\pm}$	Reaction rate constant activation Energy (J/mol)
E_R	Film resistance activation energy (J/mol)
h	Cell heat transfer coefficient (W/cm^2-K)
F	Faraday's constant (C/mol)
I	Current (A)
$K^{\pm}$	Reaction rate constant (cm$^{2.5}$/mol$^{0.5}$/s)
$K_{ref}^{\pm}$	Reaction rate constant at T_{ref} (cm$^{2.5}$/mol$^{0.5}$/s)
$L^{\pm}$	Cell length (cm)
r	Radial coordinate (cm)
R	Solid active particle Radius (cm)
$\bar{R}$	Universal Gas Constant (J/mol-K)
$R_{f,ref}$	Contact film resistance at T_{ref} (Ω)

T	Temperature (K)
T_{ref}	Reference temperature (K)
T_∞	Ambient emperature (K)
$U^{\pm}$	Open circuit voltage (V)
$\alpha^{\pm}$	Charge transfer coefficient
ρ	Cell density (g/cm^3)
v	Cell volume (cm^3)
C_p	Specific heat capacity (J/g-K)

Superscript

$\pm$	positive/negative electrode

REFERENCES

[1] Saha, B., Goebel, K., Poll, S., and Christophersen, J., 2007. "An integrated approach to battery health monitoring using bayesian regression and state estimation". In 2007 IEEE Autotestcon, pp. 646-653.

[2] Ng, K. S., Moo, C., Chen, Y., and Hsieh, Y., 2009. "Enhanced coulomb counting method for estimating state-of-charge and state-of-health of lithium-ion batteries". *Applied Energy*, vol. 86, no. 9, pp. 1506-1511.

[3] Plett, G. L., 2004. "Extended Kalman filtering for battery management systems of LiPB-based HEV battery packs: Part 3. State and parameter estimation". *Journal of Power sources*, vol. 134, no. 2, pp. 277-292.

[4] Kim, Il-Song, 2010. "A Technique for Estimating the State of Health of Lithium Batteries Through a Dual-Sliding-Mode Observer". *IEEE Transactions on Power Electronics*, vol.25, no.4, pp.1013-1022.

[5] Chaturvedi, N. A., Klein, R., Christensen, J., Ahmed, J., and Kojic, A., 2010. "Algorithms for Advanced Battery-Management Systems". *IEEE Control Systems Magazine*, vol.30, no.3, pp.49-68.

[6] Doyle, M., Fuller, T. F., and Newman, J., 1993. "Modeling of galvanostatic charge and discharge of the lithium/polymer/insertion cell". *Journal of the Electrochemical Society*, vol. 140, no. 6, pp. 1526-1533.

[7] Smith, K. A., Rahn, C. D., and Wang, C., 2010. "Model-based electrochemical estimation and constraint management for pulse operation of lithium ion batteries". *IEEE Transactions on Control Systems Technology*, vol. 18, no. 3, pp. 654-663.

[8] Klein, R.; Chaturvedi, N.A.; Christensen, J.; Ahmed, J.; Findeisen, R.; Kojic, A., 2013. "Electrochemical Model Based Observer Design for a Lithium-Ion Battery". *IEEE Transactions on Control Systems Technology*, vol.21, no. 2, pp. 289-301.

[9] Santhanagopalan, S., and White, R. E., 2006. "Online estimation of the state of charge of a lithium ion cell". *Journal of Power Sources*, vol. 161, no. 2, pp. 1346-1355.

[10] Domenico, D., Stefanopoulou, A., and Fiengo, G., 2010. "Lithium-ion battery state of charge and critical surface charge estimation using an electrochemical model-

based extended Kalman filter". *ASME Journal of Dynamic Systems, Measurement, and Control*, vol. 132, no. 6, pp. 061302.

[11] Moura, S. J., Chaturvedi, N. A., and Krstic, M., 2012. "PDE estimation techniques for advanced battery management systems—Part I: SOC estimation". In 2012 American Control Conference (ACC), pp. 559-565.

[12] Dey, S., and Ayalew, B., "Nonlinear Observer Designs for State-of-Charge Estimation of Lithium-ion Batteries". In 2014 American Control Conference (ACC), pp.248-253.

[13] Dey, S., Ayalew, B., and Pisu. P., 2015. "Nonlinear Robust Observers for State-of-Charge Estimation of Lithium-ion Cells Based on a Reduced Electrochemical Model". *IEEE Transactions on Control System Technology*, vol. 23, no. 5, pp. 1935-1942.

[14] Samadi, M. F., Alavi, S. M., and Saif, M., 2013. "Online state and parameter estimation of the Li-ion battery in a Bayesian framework". In 2013 American Control Conference (ACC), pp. 4693-4698.

[15] Schmidt, A. P., Bitzer, M., Imre, Á. W., and Guzzella, L., 2010. "Model-based distinction and quantification of capacity loss and rate capability fade in Li-ion batteries". *Journal of Power Sources*, vol. 195, no. 22, pp. 7634-7638.

[16] Fang, H., Wang, Y., Sahinoglu, Z., Wada, T., and Hara, S., 2014. "State of charge estimation for lithium-ion batteries: An adaptive approach". *Control Engineering Practice*, vol. 25, pp. 45-54.

[17] Moura, S. J., Chaturvedi, N. A., and Krstic, M., 2013. "Adaptive PDE Observer for Battery SOC/SOH Estimation via an Electrochemical Model". *ASME Journal of Dynamic Systems, Measurement, and Control*, vol. 136, no. 1.

[18] Wang, Y., Fang, H., Sahinoglu, Z., Wada, T. and Hara, S., 2014. "Adaptive Estimation of the State of Charge for Lithium-Ion Batteries: Nonlinear Geometric Observer Approach," *IEEE Transactions on Control Systems Technology*, available online.

[19] Dey, S., Ayalew, B., and Pisu, P., 2014. "Combined estimation of State-of-Charge and State-of-Health of Li-ion battery cells using SMO on electrochemical model." In 13th International Workshop on Variable Structure Systems, Nantes, France, June 29-July 2, pp. 1-6.

[20] Dey, S., Ayalew, B., and Pisu, P., 2014. "Adaptive Observer Design for a Li-Ion Cell Based on Coupled Electrochemical-Thermal Model." In ASME 2014 Dynamic Systems and Control Conference, pp. V002T23A001.

[21] Guo, M., Sikha, G., and White, R.E., 2011. "Single-particle model for a lithium-ion cell: thermal behavior". *Journal of The Electrochemical Society,* vol. 158, no. 2, pp. A122-A132.

[22] Tanim, T. R., Rahn, C. D., and Wang, C. Y., 2015. "A Temperature Dependent, Single Particle, Lithium Ion Cell Model Including Electrolyte Diffusion," *ASME Journal of Dynamic Systems, Measurement, and Control,* vol. 137, no. 1, pp. 011005.

[23] Lin, X., Perez, H. E., Siegel, J. B., Stefanopoulou, A. G., Li, Y., Anderson R. D., Ding, Y., and Castanier, M. P., 2013. "Online Parameterization of Lumped Thermal Dynamics in Cylindrical Lithium Ion Batteries for Core Temperature Estimation and Health Monitoring". *IEEE Transactions on Control Systems Technology*, vol.21, no.5, pp.1745-55.

[24] Hermann, R., and Krener, A, 1977. "Nonlinear Controllability and Observability," *IEEE Transactions on Automatic Control*, vol. 22, no. 5, pp. 728-740, 1977.

[25] Utkin, V., Guldner, J., and Shi, J., 1999. *Sliding mode control in electromechanical systems*. CRC press.

[26] Julier, S. J., and Uhlmann, J. K., 1996. "A general method for approximating nonlinear transformations of probability distributions." Robotics Research Group, Department of Engineering Science, University of Oxford, UK, Technical Report, 1996.

[27] Xiong, K., Zhang, H., and Chan, C., 2006. "Performance evaluation of UKF-based nonlinear filtering," *Automatica*, vol. 42, no. 2, pp. 261-270.

[28] Agubra, Victor, and Jeffrey Fergus, 2013. "Lithium ion battery anode aging mechanisms," *Materials*, vol. 6, no. 4, pp. 1310-1325.

[29] Ratnakumar, B.V., and Smart, M.C., 2010, "Lithium plating behavior in lithium-ion cells," *Journal of The Electrochemical Society*, vol. 25, pp. 241–252.

[30] Alavi, S. M. M., Samadi, M. F., and Saif, M., 2013. "Plating Mechanism Detection in Lithium-ion batteries, by using a particle-filtering based estimation technique," In Proceedings of 2013 American Control Conference, pp. 4356-4361.

[31] Harris, S.J., Timmons, A., Baker, D.R., Monroe, C., 2010. "Direct in situ measurements of Li transport in Li-ion battery negative electrodes," *Chemical Physics Letters*, vol. 485, pp. 265-274.

[32] Speltino, C., Domenico, D. Di, Stefanopoulou, A., and Fiengo, G., 2009. "Experimental identification and validation of an electrochemical model of a lithium-ion battery." In Proceedings of 2009 IEEE European Control Conference.

[33] Siegel, J. B., Lin, X., Stefanopoulou, A. G., Hussey, D. S., Jacobson, D. L., and Gorsich, D., 2011. "Neutron imaging of lithium concentration in LFP Pouch cell battery". *Journal of the Electrochemical Society*, vol.158, no.5, pp. A523 – A529.

[34] Dey, S., Ayalew, B., and Pisu, P., 2015. "Estimation of Lithium-ion Concentrations in Both Electrodes of a Lithium-ion Battery Cell." In ASME 2015 Dynamic Systems and Control Conference, pp. V002T26A001.

[35] Dey, Satadru, Ayalew, B., and Pisu, P., 2015. "Nonlinear Adaptive Observer for a Lithium-Ion Battery Cell Based on Coupled Electrochemical–Thermal Model." *ASME Journal of Dynamic Systems, Measurement, and Control*, vol. 137, no. 11, 111005.

[36] Rahn, Christopher D., and Chao-Yang Wang. *Battery systems engineering*. John Wiley & Sons, 2013.

[37] Prada, E., Di Domenico, D., Creff, Y., Bernard, J., Sauvant-Moynot, V., & Huet, F. (2012). "Simplified electrochemical and thermal model of LiFePO4-graphite Li-ion batteries for fast charge applications." *Journal of the Electrochemical Society*, vol. 159, no. 9, pp. A1508-A1519.

Table Caption List

Table 1   Bulk SOC estimation error under parametric uncertainties

Figure Captions List

Fig. 1   Schematic of the single particle model (SPM)

Fig. 2   The functions $\mathbf{U_P}$, $\mathbf{U_N}$, $\mathbf{U_P^D}$ and $\mathbf{U_N^D}$ for LiCoO2-Graphite chemistry [21]

Fig. 3   Estimation Scheme

Fig. 4   Temperature and voltage tracking

Fig. 5   Surface concentration tracking by Observer II

Fig. 6   Negative and positive electrode bulk SOC estimation performance

Fig. 7   Pseudo-measurement and capacity estimation performance

Fig. 8   Estimation performance of the observer-based scheme under dynamic discharge profile

Fig. 9   Comparison of the estimation performance "with the conservation assumption" and the proposed scheme

Fig. 10   Capacity fade tracking performance

Fig. 11   Bulk SOC estimation performance under Lithium plating (with C/10 charging and ambient temperature -20$^{\mathrm{o}}$C). The plating is injected at t=600 sec

Fig. 12   Lithium plating detection performance with C/10 charging and ambient temperature -20$^{\mathrm{o}}$C. The plating is injected at t=600 sec and the Li-ion extraction rate from positive electrode (E_P) goes beyond the maximum limit

Fig. 13   Bulk SOC estimation error under different level of temperature measurement noise

Fig. 14   Bulk SOC estimation error under parametric uncertainties ($R_{f,ref}$, h and C_p)

Fig. 15   Estimation error under zero current. The current is made to zero at 1000 sec.

Table 1: Bulk SOC estimation error under parametric uncertainties

Parametric Uncertainties	Bulk SOC Estimation Error	
	Negative Electrode	Positive Electrode
50% deviation in $D_{s,ref}^{-}$	4%	2%
50% deviation in $D_{s,ref}^{+}$	3%	6%
50% deviation in a_s^{-}	5%	2%
50% deviation in a_s^{+}	3%	7%

Figure 1. Schematic of the single particle model (SPM)
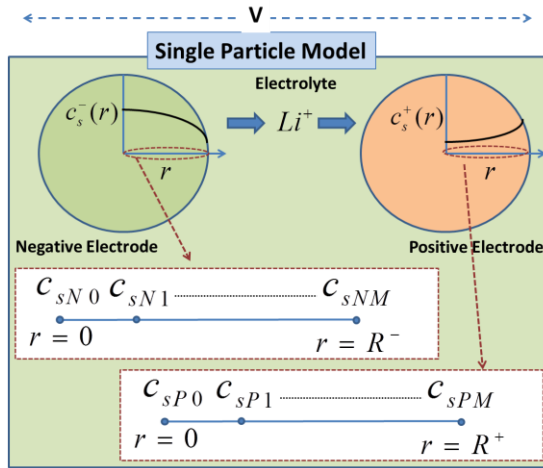
Figure 2: The functions U_P, U_N, U_P^D and U_N^D for LiCoO2-Graphite chemistry [21]
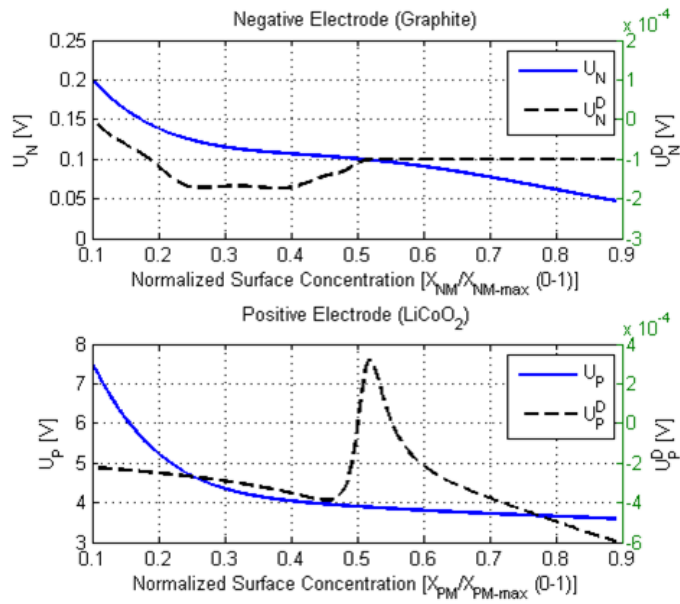
Figure 3: Estimation Scheme
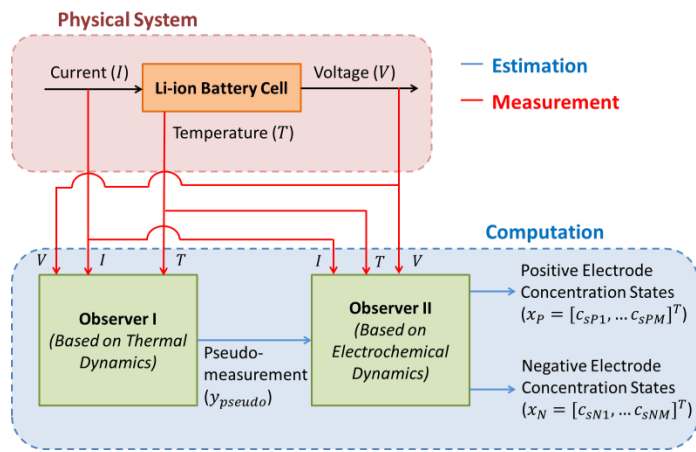
Figure 4: Temperature and voltage tracking
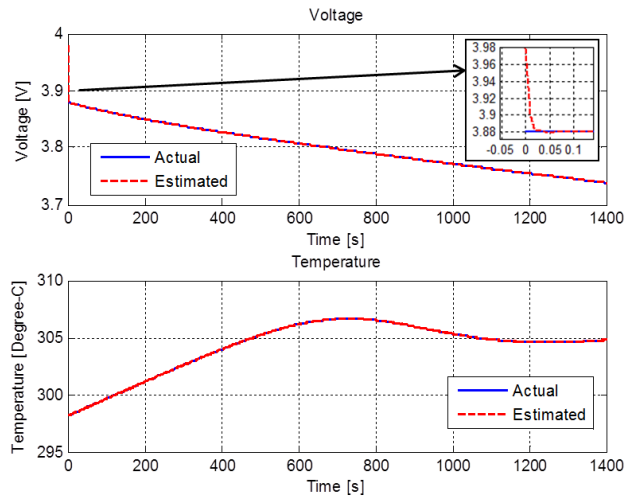
Figure 5: Surface concentration tracking by Observer II
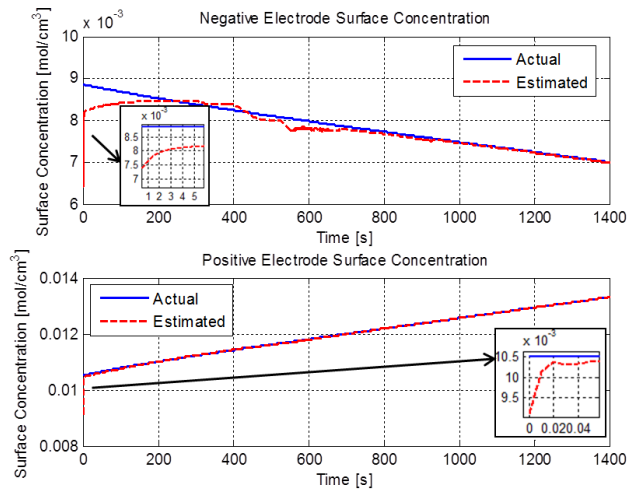
Figure 6: Negative and positive electrode bulk SOC estimation performance
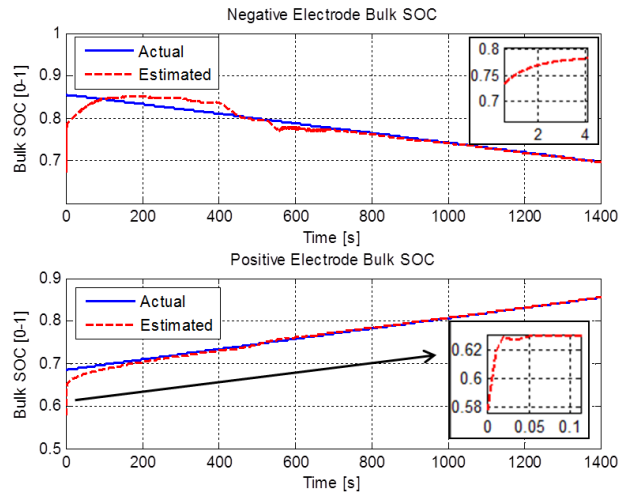
Figure 7: Pseudo-measurement and capacity estimation performance
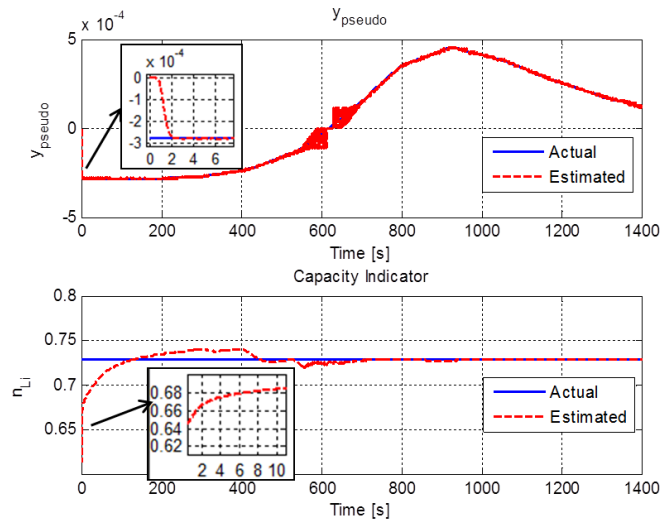
Figure 8: Estimation performance of the observer-based scheme under dynamic discharge profile
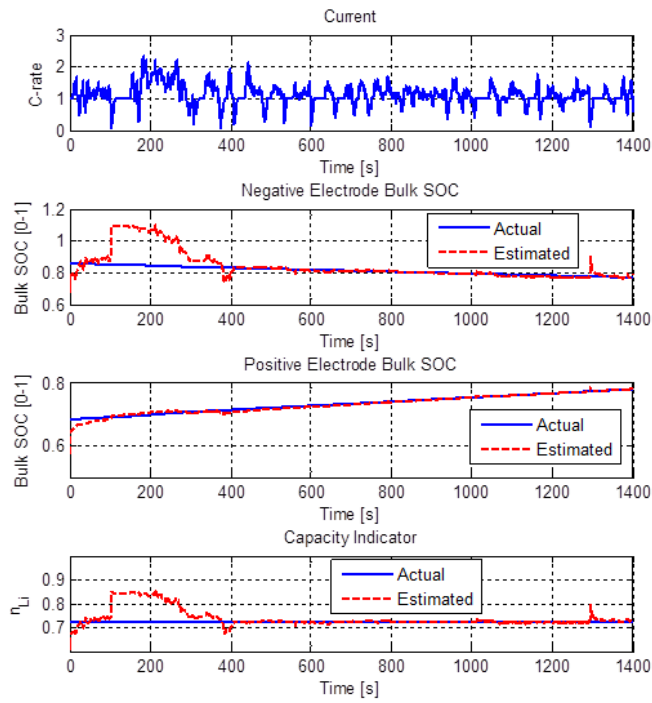
Figure 9: Comparison of the estimation performance "with the conservation assumption" and the proposed scheme
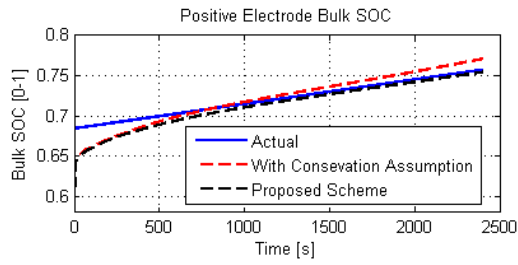
Figure 10: Capacity fade tracking performance
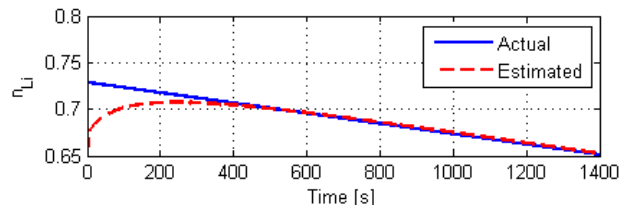
Figure 11: Bulk SOC estimation performance under Lithium plating (with C/10 charging and ambient temperature -20°C). The plating is injected at t=600 sec
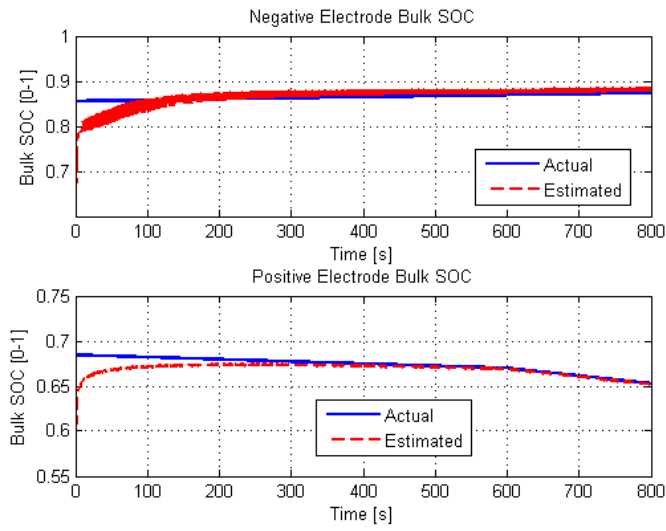
Figure 12: Lithium plating detection performance with C/10 charging and ambient temperature -20°C. The plating is injected at t=600 sec and the Li-ion extraction rate from positive electrode (E_P) goes beyond the maximum limit
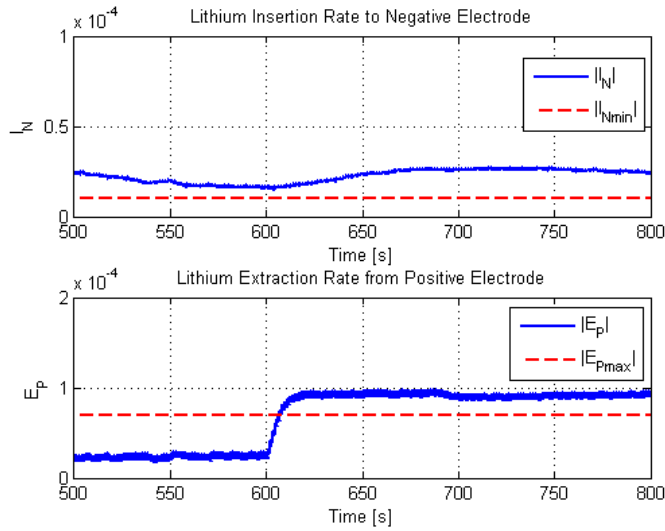
Figure 13: Bulk SOC estimation error under different level of temperature measurement noise
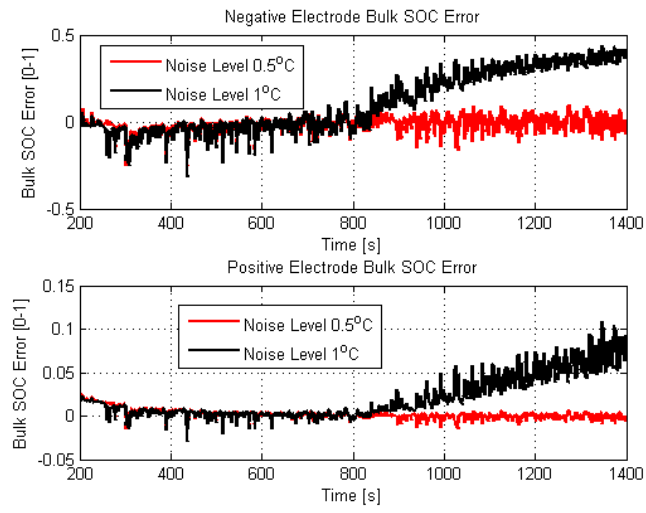
Figure 14: Bulk SOC estimation error under parametric uncertainties ($R_{f,ref}$, h and C_p)
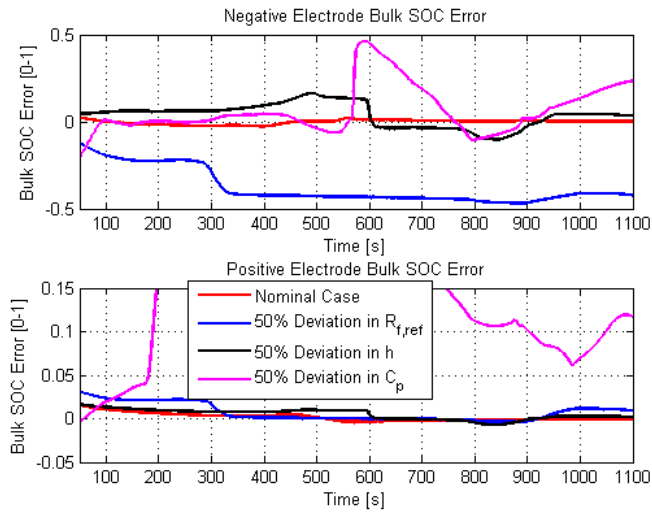
Figure 15: Estimation error under zero current. The current is made to zero at 1000 sec.